Modulated Model Predictve Control (M^2PC) for a 3-Phase Active Rectifier

Luca Tarisciotti*, Pericle Zanchetta,
Alan Watson, Jon Clare, Marco Degano
Department of Electrical and Electronic Engineering
University of Nottingham
Nottingham, UK
* eexlt1@nottingham.ac.uk

Stefano Bifaretti
Department of Electronic Engineering
University of Rome Tor Vergata
Rome, Italy

***Abstract*— One of the main issues of Model Predictive Control applied to Power Electronics Converters is the availability of selecting only a limited amount of converter switching states for waveforms generation, thus requiring a high switching frequency in order to achieve reasonable harmonic content. The nature of this control method also results in variable switching frequency, making filter design complicated. In order to overcome these issues, whilst still preserving all of the desired characteristics of MPC, this paper presents a novel Modulated Model Predictive Control, with the aim of obtaining a modulated waveform at the output of the converter without implementing an explicit modulation scheme. The proposed control technique is applied for the current control of a 2-Level 3-Phase inverter and validated, through simulations performed in Matlab/PLECS, in comparison with the classical Model Predictive Control, Dead Beat Control and PI control in a stationary reference frame. The control has been implemented and experimentally validated on a 2-Level 3-Phase active rectifier and compared to a traditional Model Predictive Control.**

I. INTRODUCTION

In the past decade, Model Predictive Control (MPC) has been widely proposed as a promising solution for the control of power converters due to several advantages, such as fast dynamic response, lack of modulator, easy inclusion of nonlinearities and constraints of the system, possibility to incorporate nested control loops into a single loop and the flexibility to include other system requirements in the controller [1]–[5]. MPC considers a model of the system in order to predict its future behavior over a time horizon. Based on this model, MPC solves an optimization problem where a sequence of future actuation demands are obtained by minimizing a cost function, which represents the desired behavior of the system. The best performing actuation is then applied and the calculations are repeated every sample period. Power converters are systems with a finite number of states, given by the possible combinations of the state of the switching devices; the MPC optimization problem can be simplified and reduced to the prediction of the system behaviour for each possible state. Then, each prediction is evaluated using the cost function and the state that minimizes it, is selected [1]. This approach, named Finite Control Set Model Predictive Control (FCS-MPC), has been successfully applied for the current control in a three-phase converter [1]–[3], [6] in a matrix converter [7]–[9], for the power control in an active front end rectifier [5] or in the torque and flux control of an induction machine [10]–[13]. However, one of the main drawbacks of FCS-MPC is that, because of the absence of a modulator, the control can choose only among a limited amount of converter switching states and apply one for the entire switching period. This generates a larger ripple in the system waveforms, which in turn requires an increased (and variable) switching frequency in comparison to other control solutions. Several solutions are proposed in literature to modify the pulse pattern of FCS-MPC [14], improve the applied vector sequence [15], introduce a modulation scheme inside the MPC algorithm [16]–[18], or increase the MPC prediction horizon [19]–[22]. In [16] an analytical solution to the switching times calculation problems is provided, whilst in [17], [18] also a Space Vector Modulation technique (SVM) is applied to the MPC current control of a six-phase inverter to feed an Asymmetrical Dual Three-Phase Induction Machine. In such approaches, the duty cycles are calculated by solving an optimization problem; then, the optimal control action is determined in order to track the desired reference with minimal error. However, multi-objective control becomes rather complex since it would require a solution for a multidimensional optimization problem to be derived. In [19]–[22] a method is presented which increases of the prediction horizon of FCS-MPC improves the control performances; the main drawback in this case is that the increased numbers of possible converter states results in a larger computational effort on the control hardware. Depending on the available calculation power, such a solution may not be feasible in real systems. In order to overcome this limitation, a novel approach, named Modulated Model Predictive Control (M^2PC), is proposed in this paper; it allows the retention of all the desired characteristics of FCS-MPC as a multi-objective control strategy, but produces an increased performance in terms of power quality. A similar solution has already been proposed in [23], [24] where the ratio betweeen cost function for different converter states has been used to include a suitable modulation scheme inside the cost function minimization algorithm. However, this technique has been specifically designed for high power system where a limited amount of commutations are applied. In the proposed work the switching instants are calculated considering an inverse SVM technique.

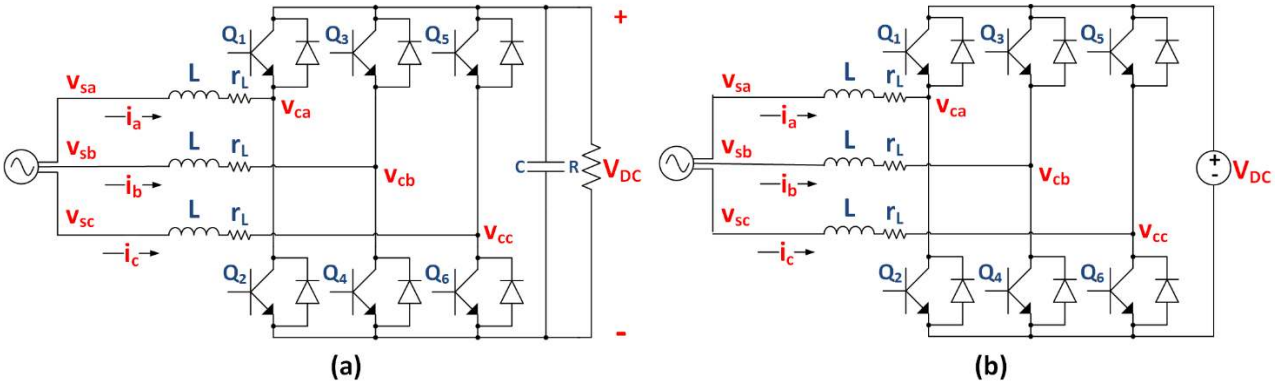

Figure 1. Proposed 3-phase, 2 level Active Front-End: (a) Active rectifier configfuration (b) Inverter configuration.

By knowing a priori the desired active vectors to be applied, the duty cycles are calculated for any possible converter state and used to weight the cost function. The proposed control solution is demonstrated and tested for the simple case of the AC current control of a grid connected 3-phase converter, shown in figure 1, in order to better compare and contrast its performance against different control techniques, such as Proportional Integral (PI) control in a synchronous reference frame [25], [26], Dead Beat Control (DBC) [27]–[29], and traditional MPC.

II. CONVERTER DESCRIPTION

A 2-Level, 3-Phase bidirectional AC/DC converter is shown in figure 1. By using similar control schemes is possible to control both operational modes, differing only in the need of an additional controller for the DC-Link voltage using the rectifier structure.

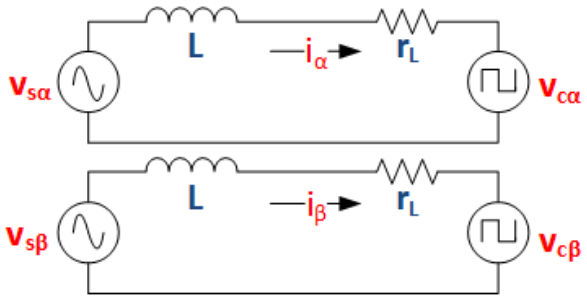

Figure 2. Equivalent (α,β) model of the Active Front-End.

Using the Clarke's transform shown below, where x is a voltage or a current, it is possible to obtain a two phase (αβ) representation of the 3-Phase circuit shown in figure 2.

$$x_\alpha = \frac{2}{3}[x_a - (x_b + x_c)] \tag{1}$$

$$x_\beta = \frac{\sqrt{3}}{3}(x_b + x_c) \tag{2}$$

Considering that the voltages produced from the converter are related to the state of the switching devices, S_α and S_β, and the DC-Link voltage, V_{DC}, according to the following equations, the Active Front-End can produce 8 different voltage vectors on the (αβ) plane, 6 active vectors and 2 zero vectors.

$$v_{c\alpha}(t) = S_\alpha(t)V_{DC} \tag{3}$$

$$v_{c\beta}(t) = S_\beta(t)V_{DC} \tag{4}$$

S_α and S_β represent the selected converter state in the αβ plane, i.e. intrinsically discrete. In table I the values of S_α, S_β for any possible switching device configuration are shown.

$$\begin{cases} \dfrac{di_\alpha(t)}{dt} = \dfrac{1}{L}[v_{s\alpha}(t) - S_\alpha(t)V_{DC}] - \dfrac{r_l}{L}i_\alpha(t) \\ \dfrac{di_\beta(t)}{dt} = \dfrac{1}{L}[v_{s\beta}(t) - S_\beta(t)V_{DC}] - \dfrac{r_l}{L}i_\beta(t) \end{cases} \tag{5}$$

A discrete time model is obtained from (5) assuming that the system variables are considered constant during the sampling interval T_s.

$$\begin{cases} i_\alpha(t_k + T_s) = K_1 i_\alpha(t_k) + K_2[v_{s\alpha}(t_k) - S_\alpha(t_k)V_{DC}] \\ i_\beta(t_k + T_s) = K_1 i_\alpha(t_k) + K_2[v_{s\beta}(t_k) - S_\beta(t_k)V_{DC}] \end{cases} \tag{6}$$

In (6) t_k is the actual time instant and K_1, K_2 are two constants defined in (7) and (8) where L is the line inductance and r_l is the inductor parasitic resistance..

$$K_1 = e^{-\frac{r_l}{L}T_s} \approx 1 - \frac{r_l}{L}T_s \tag{7}$$

$$K_2 = \frac{1}{r_l}\left(1 - e^{-\frac{r_l}{L}T_s}\right) \approx \frac{T_s}{L} \tag{8}$$

In order to obtain a fair evaluation of the proposed control technique, the M^{2}PC controller is compared MPC and a complete control scheme suitable for both controllers is proposed.

TABLE I. SWITCHING STATES AND EQUIVALENT (α,β) COMPONENTS

S	Q_1 / Q_2	Q_3 / Q_4	Q_5 / Q_6	S_α	S_β
0	0 / 1	0 / 1	0 / 1	0	0
1	1 / 0	0 / 1	0 / 1	2⁄3	0
2	1 / 0	1 / 0	0 / 1	1⁄3	√3⁄3
3	0 / 1	1 / 0	0 / 1	-1⁄3	√3⁄3
4	0 / 1	1 / 0	1 / 0	-2⁄3	0
5	0 / 1	0 / 1	1 / 0	-1⁄3	-√3⁄3
6	1 / 0	0 / 1	1 / 0	1⁄3	-√3⁄3
7	1 / 0	1 / 0	1 / 0	0	0

III. OVERALL CONTROL SCHEME

The overall control scheme for the converter is shown in figure 3 where the absence of a modulation scheme is clear. The aim of the method is to control the AC current; in the case of active rectifier configuration the current reference have to be chosen in order to regulate the DC link voltages at the required reference. A control loop with a proportional Integral (PI) controller is used to achieve this aim and provide a current reference for M^{2}PC.

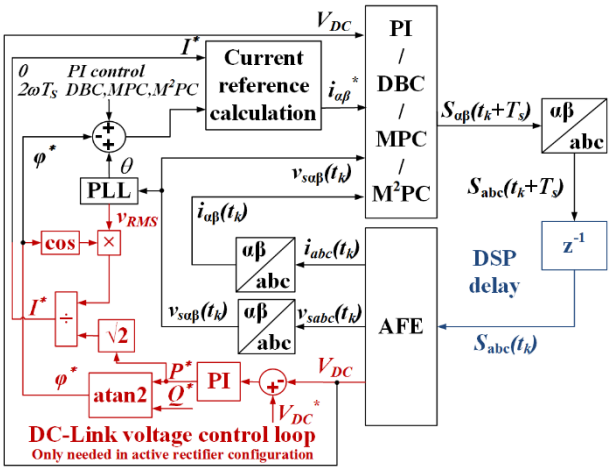

Figure 3. Overall control block scheme.

The current reference is calculated as in (9) and (10), where I^* represents the desired current amplitude and φ^* is the desired phase shift between AC current and supply voltage.

$$i_\alpha{}^*(t_k + 2T_s) = I^* \cos(\theta + 2T_s - \varphi^*) \quad (9)$$

$$i_\beta{}^*(t_k + 2T_s) = I^* \sin(\theta + 2T_s - \varphi^*) \quad (10)$$

To obtain the φ^* a PLL is also needed to measure the supply voltage phase angle θ [30]. For the case of the active rectifier configuration the current reference is calculated based on the desired active and reactive power, P^* and Q^*, respectively.

$$\varphi^* = \text{atan2}(Q^*, P^*) \quad (11)$$

$$I^* = \frac{P^*}{\sqrt{2} v_{rms} \cos(\varphi^*)} \quad (12)$$

IV. OTHER CONTROL TECHNIQUES

M2PC has been compared with three different control techniques, already proposed in literature; a brief description of these control techniques is provided in the following paragraphs.

A. PI control in synchronous reference frame

A classical control scheme based on the current control in synchronous reference frame [25], [26] is shown in Figure 4. The current on the *d*-axis and *q*-axis, respectively I_d and I_q, are regulated to the desired references $I_d{}^*$ and $I_q{}^*$ using two PI controllers. Feed-forward terms are also implemented to improve the overall current control performance. A SVM technique used to convert the demanded converter voltages into pulsed gate signals.

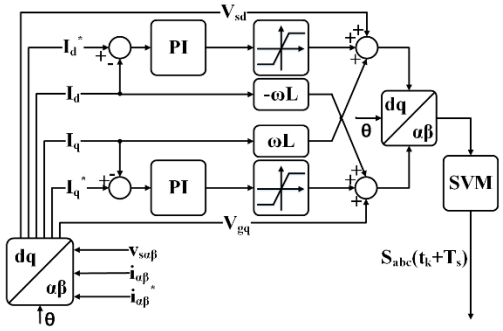

Figure 4. PI control in synchronous reference frame block scheme.

B. Dead-Beat Control

Dead-Beat control [27]–[29] is based on the prediction of the system response to a change in control variables in order to achieve (ideally) zero error in the next one, two or more sampling periods. The output of this control is an average value (i.e. continuous) and it is chosen by attempting to gain a current at the next sampling instant equal to the desired reference. In real control systems if the computational time, usually fixed at one sampling interval, is not taken into account, the control action would be performed with a delay of one sampling interval. To compensate for the aforementioned delay, the two sample step prediction proposed in [31] is used, thus results in the following Dead Beat control law

$$S_\alpha{}^*(t_k + T_s) = \frac{1}{V_{DC}} \left\{ v_{S\alpha}(t_k + T_s) + \left[\frac{K_1}{K_2} i_\alpha(t_k) + - \frac{1}{K_2} i_\alpha{}^*(t_k + 2T_s) \right] \right\} \quad (13)$$

$$S_\beta{}^*(t_k + T_s) = \frac{1}{V_{DC}} \left\{ v_{S\beta}(t_k + T_s) + \left[\frac{K_1}{K_2} i_\beta(t_k) + - \frac{1}{K_2} i_\beta{}^*(t_k + 2T_s) \right] \right\} \quad (14)$$

A modulator is needed to apply desired output voltage to the converter. Applying this control method, the current will follow ideally the desired reference with zero error at the next sampling period.

C. Model Predictive Control

Finite Control Set Model Predictive Control is based on the prediction of the system response to a change in control variables in order to achieve a minimum error in the next one, two or more sampling periods. The output of this control is a discrete value that can be directly applied to control the converter and it is chosen by minimizing a cost function that represents the error between the current and the desired reference. Applying FCS-MPC to control the AC current, the desired reference is tracked with minimum error at the next sampling period. In order to allow the implementation using a DSP or microcontroller, the discrete time model of (6) is considered. The computational delay introduced by the implementation can be represented as a delay of one sampling interval, T_s, on the applied converter voltage $v_{c\alpha}$, $v_{c\beta}$, i.e. on S_α, S_β.

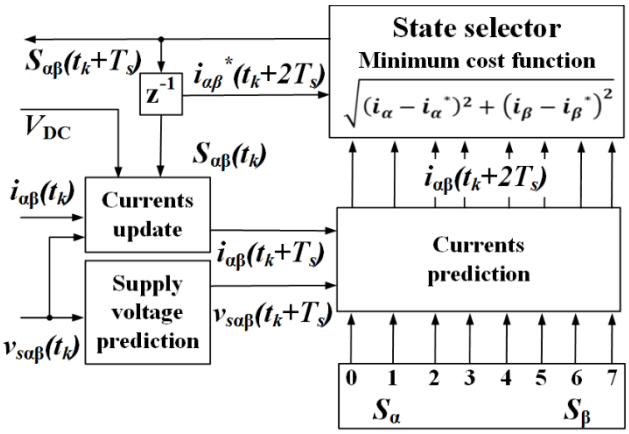

Figure 5. MPC block scheme.

To compensate the delay described above two steps of prediction are needed. In fact, assuming that $S_\alpha(t_k)$, $S_\beta(t_k)$, calculated during the previous sampling interval and applied to the converter whilst computing their new values, the first prediction step just updates the i_α, i_β values using the previously calculated converter state.

$$i_\alpha(t_k + T_s) = K_1 i_\alpha(t_k) + K_2[v_{s\alpha}(t_k) - S_\alpha(t_k)V_{DC}] \quad (15)$$

$$i_\beta(t_k + T_s) = K_1 i_\alpha(t_k) + K_2\left[v_{s\beta}(t_k) - S_\beta(t_k)V_{DC}\right] \quad (16)$$

The current update does not represent an extension in the prediction horizon; the cost function is not calculated and the predictive optimization problem is not solved at the time instant $t_k + T_s$. Thus, the proposed FCS-MPC control can be considered as having a one-step prediction horizon. Once the current has been updated a current prediction, based on the following equation,

$$i_\alpha(t_k + 2T_s) = K_1 i_\alpha(t_k + T_s) + \\ + K_2[v_{s\alpha}(t_k + T_s) - S_\alpha(t_k + T_s)V_{DC}] \quad (17)$$

$$i_\beta(t_k + 2T_s) = K_1 i_\alpha(t_k + T_s) \\ + K_2\left[v_{s\beta}(t_k + T_s) - S_\beta(t_k + T_s)V_{DC}\right] \quad (18)$$

is calculated for any possible converter state, i.e. for any possible value of S_α, S_β and it is chosen to be applied the value of S_α, S_β that minimize the following cost function, at the time instant $t_k + 2T_s$.

$$G = \sqrt{(i_\alpha - i_\alpha^*)^2 + \left(i_\beta - i_\beta^*\right)^2} \quad (19)$$

where i_α^*, i_β^* are the desired current references. Figure 5 shows the MPC block scheme where the supply voltage prediction is calculated as described in [32], assuming an ideal supply voltage. The prediction horizon may be extended, as proposed in [19]–[22], in order to improve control performance; however, the computational complexity of FCS-MPC increases exponentially with the prediction horizon. Figure 6 shows the execution time of the proposed FCS-MPC on a Texas Instrument C6713 DSP when an interrupt time of 20kHz is selected in order to make available 50µs for the control algorithm execution. Selecting a prediction horizon of one sampling interval, the FCS-MPC program needs 27.4µs to be executed, of which 3.2µs is required to calculate currents predictions, cost functions and find the minimum value of the cost function G.

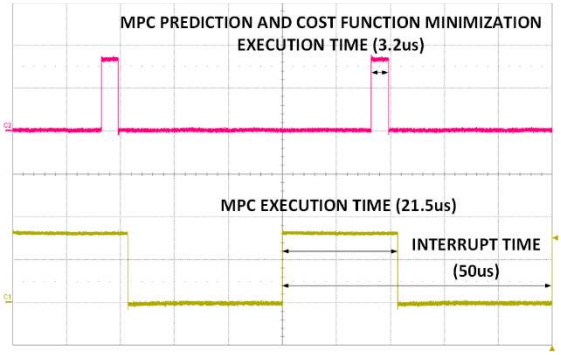

Figure 6. FCS-MPC execution time.

By using this data to predict the computational time of an extended horizon controller, it is possible to deduce a potential limitation in the number of sampling periods which can be included. Thi is based on the need to ensure that all computations are carried out during a single interrupt period. Clearly, for a 20kHz interrupt a horizon of two is the maximum can be applied. This can be improved with a faster hardware but a greater financial cost.

TABLE II. ESTIMATED FCS-MPC EXECUTION TIME FOR DIFFERENT PREDICTION HORIZONS.

PREDICTION HORIZON	NUMBER OF ITERATIONS	MPC EXECUTION TIME	TOTAL EXECUTION TIME
1	8	3.2 us	21.5 us
2	64	25.6 us	43.9 us
3	512	204.8 us	200.7 us
4	4096	1638.4 us	1659.9 us
5	32768	13107.2 us	13128.7 us

V. MODULATED MODEL PREDICTIVE CONTROL

Modulated Model Predictive Control (M^2PC) includes a suitable modulation scheme in the cost function minimization of the MPC alghorithm. To avoid increasing excessively the complexity of the controller [15], [16], especially in the case of multi-objective cost functions, M^2PC is based on the evaluation of the cost function for a selected number of states. Figure 7 shows the block scheme of M^2PC. Clearly, the supply voltage prediction is also required and calculated as described in [33], assuming an ideal supply voltage. It is also necessary to calculate a converter voltage reference to provide the correct time intervals related to the selected active and the zero vectors. The two active vectors are selected between all the possible couples of adjacent vectors using a cost function minimization based on the current predictions and the duty cycles d_0, d_1, d_2, related to the selected vectors. A Space Vector Modulation (SVM) scheme is adopted and 2 active vectors and two zero vectors are applied during every sampling interval. A switching pattern, such as the one shown in figure 8, is applied, where the vectors S_1 and S_2 from table I are selected to be applied respectively for a time d_1T_s and d_2T_s.

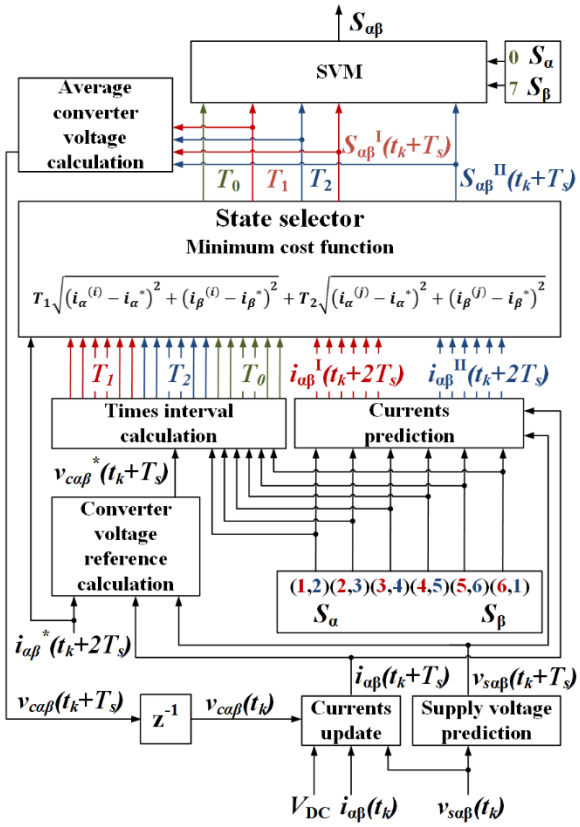

Figure 7. M²PC block scheme.

The two zero vectors, respectively S_0 and S_7, are both applied during the sampling interval for a total time d_0T_s.

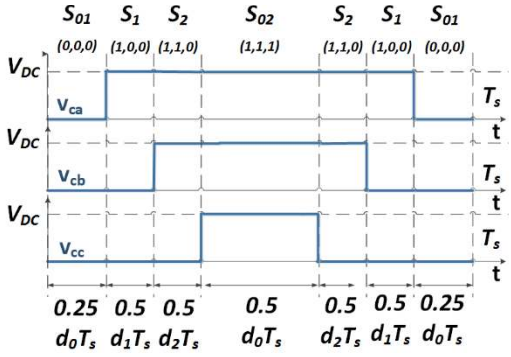

Figure 8. M²PC typical switching pattern.

A. AC side current update

The M²PC algorithm starts, as for MPC, with an AC side current update in order to compensate the delay introduced by the DSP.

$$i_\alpha(t_k+T_s) = K_1 i_\alpha(t_k) + K_2[v_{s\alpha}(t_k) - V_{c\alpha}(t_k)] \quad (20)$$

$$i_\beta(t_k+T_s) = K_1 i_\alpha(t_k) + K_2[v_{s\beta}(t_k) - V_{c\beta}(t_k)] \quad (21)$$

In this case, because of the inclusion of a modulation scheme into the control algorithm, the average voltages produced by the converter have to be considered,

$$V_{c\alpha}(t_k) = V_{DC}\left[d_1 S_\alpha{}^{I}(t_k) + d_2 S_\alpha{}^{II}(t_k)\right] \quad (22)$$

$$V_{c\beta}(t_k) = V_{DC}\left[d_1 S_\beta{}^{I}(t_k) + d_2 S_\beta{}^{II}(t_k)\right] \quad (23)$$

where $(S_\alpha{}^I, S_\beta{}^I)$ and $(S_\alpha{}^{II}, S_\beta{}^{II})$ are the two vectors selected by the M²PC algorithm and d_1, d_2 are the associated duty cycles.

B. Converter voltage reference calculation

The converter voltage reference $(v_{c\alpha}{}^*, v_{c\beta}{}^*)$ is calculated considering that the current predictions can be rewritten as

$$i_\alpha(t_k+2T_s) = i_\alpha{}^0(t_k+2T_s) - K_2 V_{c\alpha}(t_k+T_s) \quad (24)$$

$$i_\beta(t_k+2T_s) = i_\beta{}^0(t_k+2T_s) - K_2 V_{c\beta}(t_k+T_s) \quad (25)$$

where $(i_\alpha{}^0, i_\beta{}^0)$ represent the unforced evolution of the system, i.e. when a zero vector is applied and $(v_{c\alpha}, v_{c\beta})=(0,0)$.

$$i_\alpha{}^0(t_k+2T_s) = K_1 i_\alpha(t_k+T_s) + K_2 v_{s\alpha}(t_k+T_s) \quad (26)$$

$$i_\beta{}^0(t_k+2T_s) = K_1 i_\beta(t_k+T_s) + K_2 v_{s\beta}(t_k+T_s) \quad (27)$$

Then the error vector $(\Delta I_\alpha, \Delta i_\beta)$ is calculated as the difference between the current references and the currents produced from the zero vectors.

$$\Delta i_\alpha(t_k+2T_s) = i_\alpha{}^0(t_k+2T_s) - i_\alpha{}^*(t_k+2T_s) \quad (28)$$

$$\Delta i_\beta(t_k+2T_s) = i_\beta{}^0(t_k+2T_s) - i_\beta{}^*(t_k+2T_s) \quad (29)$$

Considering the control working properly is possible to assume that

$$i_\alpha(t_k+2T_s) = i_\alpha{}^*(t_k+2T_s) \quad (30)$$

$$i_\beta(t_k+2T_s) = i_\beta{}^*(t_k+2T_s) \quad (31)$$

Under the hypothesis of (30), (31) it is possible to substitute $i_\alpha{}^0$, $i_\beta{}^0$ from (24), (25) respectively into (28), (29), obtaining the desired expression of the converter voltage references.

$$V_{c\alpha}{}^*(t_k+T_s) = \frac{\Delta i_\alpha(t_k+2T_s)}{K_2} = \frac{\sqrt{G^{(0)2} - G_\beta^{(0)2}}}{K_2} \quad (32)$$

$$V_{c\beta}{}^*(t_k+T_s) = \frac{\Delta i_\beta(t_k+2T_s)}{K_2} = \frac{\sqrt{G^{(0)2} - G_\alpha^{(0)2}}}{K_2} \quad (33)$$

Eqs. (32) and (33) show that the converter voltage references can be expressed only as a function of the zero vector cost function components $G^{(0)}{}_\alpha$, $G^{(0)}{}_\beta$ of the zero vector cost function $G^{(0)}$.

$$G^{(0)} = \sqrt{\left(i_\alpha{}^{(0)} - i_\alpha{}^*\right)^2 + \left(i_\beta{}^{(0)} - i_\beta{}^*\right)^2} = \sqrt{G_\alpha^{(0)2} + G_\beta^{(0)2}} \quad (34)$$

This result allows the implementation of the modulation algorithm even in the case of multi-objective control, for example, including the DC-Link voltage control loop into the M²PC algorithm.

C. AC side current predictions

The AC side current predictions are calculated for each of the adjacent active vectors considering both vectors applied for the whole sampling interval T_s.

$$i_\alpha{}^{(i)}(t_k+2T_s) = i_\alpha{}^0(t_k+2T_s) - K_2 V_{DC} S_\alpha{}^{(i)}(t_k+T_s) \quad (35)$$

$$i_\beta{}^{(i)}(t_k + 2T_s) = i_\beta{}^0(t_k + 2T_s) - K_2 V_{DC} S_\beta{}^{(i)}(t_k + T_s) \quad (36)$$

$$i_\alpha{}^{(j)}(t_k + 2T_s) = i_\alpha{}^0(t_k + 2T_s) - K_2 V_{DC} S_\alpha{}^{(j)}(t_k + T_s) \quad (37)$$

$$i_\beta{}^{(j)}(t_k + 2T_s) = i_\beta{}^0(t_k + 2T_s) - K_2 V_{DC} S_\beta{}^{(j)}(t_k + T_s) \quad (38)$$

Where *(i,j)* can assume values, according to table I.

$$(i,j) = (1,2)\,,(2,3)\,,(3,4)\,,(4,5)\,,(5,6)\,,(6,1) \quad (39)$$

D. Time interval calculations

The duty cycles are calculated based on the converter voltage reference derived from (33) and (34) for each two active vectors defined by (39). Starting from the average converter voltages applied during one sampling interval, and imposing it equal to the converter voltage reference previously calculated for the time instant $t_k + T_s$. Solving the system of (40) is possible to calculate the duty cycles as in (41) for each pair of vectors defined by (39) as shown below.

$$\begin{cases} V_{c\alpha}{}^* = V_{DC}\left[d_1 S_\alpha{}^{(i)} + d_2 S_\alpha{}^{(j)}\right] \\ V_{c\beta}{}^* = V_{DC}\left[d_1 S_\beta{}^{(i)} + d_2 S_\beta{}^{(j)}\right] \end{cases} \quad (40)$$

$$\begin{cases} d_1 = \dfrac{1}{V_{DC}} \dfrac{V_{c\beta}{}^* S_\alpha{}^{(j)} - V_{c\alpha}{}^* S_\beta{}^{(j)}}{S_\alpha{}^{(j)} S_\beta{}^{(i)} - S_\alpha{}^{(i)} S_\beta{}^{(j)}} \\ d_2 = \dfrac{1}{V_{DC}} \dfrac{V_{c\beta}{}^* S_\alpha{}^{(i)} - V_{c\alpha}{}^* S_\beta{}^{(i)}}{S_\alpha{}^{(i)} S_\beta{}^{(j)} - S_\alpha{}^{(j)} S_\beta{}^{(i)}} \end{cases} \quad (41)$$

The zero vector cost function is used to calculate the converter voltage references. The zero vector normalized time interval can be calculated according to (42).

$$d_0 = 1 - d_1 - d_2 \quad (42)$$

E. Cost function minimization

The current prediction and the time interval calculations are executed in parallel and for each pair of vectors defined by (39) a cost function is calculated as follows, at the time instant $t_k + 2T_s$. The couple of vectors with the minimum value of *G*, named $(S_\alpha{}^I, S_\beta{}^I)$, $(S_\alpha{}^{II}, S_\beta{}^{II})$, are selected to be applied for the associated duty cycles d_1, d_2.

$$G^{(i)} = \sqrt{\left(i_\alpha{}^{(i)} - i_\alpha{}^*\right)^2 + \left(i_\beta{}^{(i)} - i_\beta{}^*\right)^2} \quad (43)$$

$$G^{(j)} = \sqrt{\left(i_\alpha{}^{(j)} - i_\alpha{}^*\right)^2 + \left(i_\beta{}^{(j)} - i_\beta{}^*\right)^2} \quad (44)$$

$$G = d_1 G^{(i)} + d_2 G^{(j)} \quad (45)$$

VI. SIMULATION RESULTS

Simulations have been carried out for both controllers in a MATLAB\PLECS environment considering the inverter configuration of figure 1a. The simulation parameters are shown in Table III where it should be noticed that, in order to increase the switching frequency, a sampling frequency equal to the double of the sample frequency of the M^{2}PC, DBC and PI control has been applied for MPC. Simulation results are shown in figure 9 for MPC and M^{2}PC. The Weighted Total Harmonic Distortion, *WTHD*, and the Total Harmonic Distortion, *THD* are calculated using the following expressions, considering a general variable *x*.

$$WTHD = \frac{1}{{x_1}^2} \sum_{n=2}^{\infty} \frac{{x_n}^2}{n^2} \quad (46)$$

$$THD = \frac{1}{{x_1}^2} \sum_{n=2}^{\infty} {x_n}^2 \quad (47)$$

TABLE III. SIMULATION PARAMETERS.

Name	Description	Value	Unit
L	Line Inductance	5	[mH]
r_l	Leakage Resistance	0.5	[Ω]
V_{DC}	DC-Link Voltage	600	[V]
V_s	Supply Voltage peak value	230	[V]
f_s	Sampling Frequency	20 (MPC) 10(PI, DBC, M^{2}PC)	[kHz]
f_{sw}	Switching Frequency	~7 (MPC) 10 (PI, DBC, M^{2}PC)	[kHz]

The current tracking of MPC (figure 9a) and M^{2}PC (figure 9e) is compared considering a step in the current references of *20A* to *60A* at time *0.0625s*. The benefits of including a modulation scheme inside the predictive algorithm is clear; in fact both controllers track the current reference effectively with a fast response but M^{2}PC presents a smoother current compared to MPC. Figure 9b and figure 9f show the supply and converter voltages, respectively for MPC and M^{2}PC, and it is clear that M^{2}PC produces a converter voltage with a constant switching frequency at *10kHz* while MPC control has a variable switching frequency lower than *10kHz*, also considering a sampling frequency of *20kHz*. The variable switching frequency of MPC produce the converter voltage spectrum of figure 9c where the harmonics are spread widely across the plot, mainly below *20kHz*. Moreover, because MPC can only apply a selected state for a time that is multiple of $1/f_s$, the *WTHD* shows a higher value compared to the one for M^{2}PC, shown in figure 9g. The converter voltage spectrum of M^{2}PC presents harmonics around the frequency multiple of $f_{sw}=f_s$. Similar results are obtained considering the current spectrum for MPC (figure 9d) and M^{2}PC (figure 9h). Clearly MPC presents a higher value of THD compared to M^{2}PC. Moreover, MPC presents a high harmonic content at frequencies below the switching frequency increasing the complexity of the line filter design, while M^{2}PC converter voltage spectrum presents harmonics only around frequencies as multiples of the switching frequency. In conclusion it can be stated that the M^{2}PC presents several advantages with respect to MPC, where the most important are: fast dynamic response, fixed switching frequency of the controller, low value of *WTHD* and *THD* and converter voltage and current harmonics concentrated around the frequencies multiple of f_{sw}. In Figure 10 the simulation results obtained with DBC and PI control in the synchronous reference frame are presented. DBC shows similar results compared with M^{2}PC, whilst the PI control has a slower transient response as expected. Clearly an optimisation of the PI control may be carried out to improve the synchronous reference frame control transient response. However, M^{2}PC presents the capability of include several control target in the same control loop.

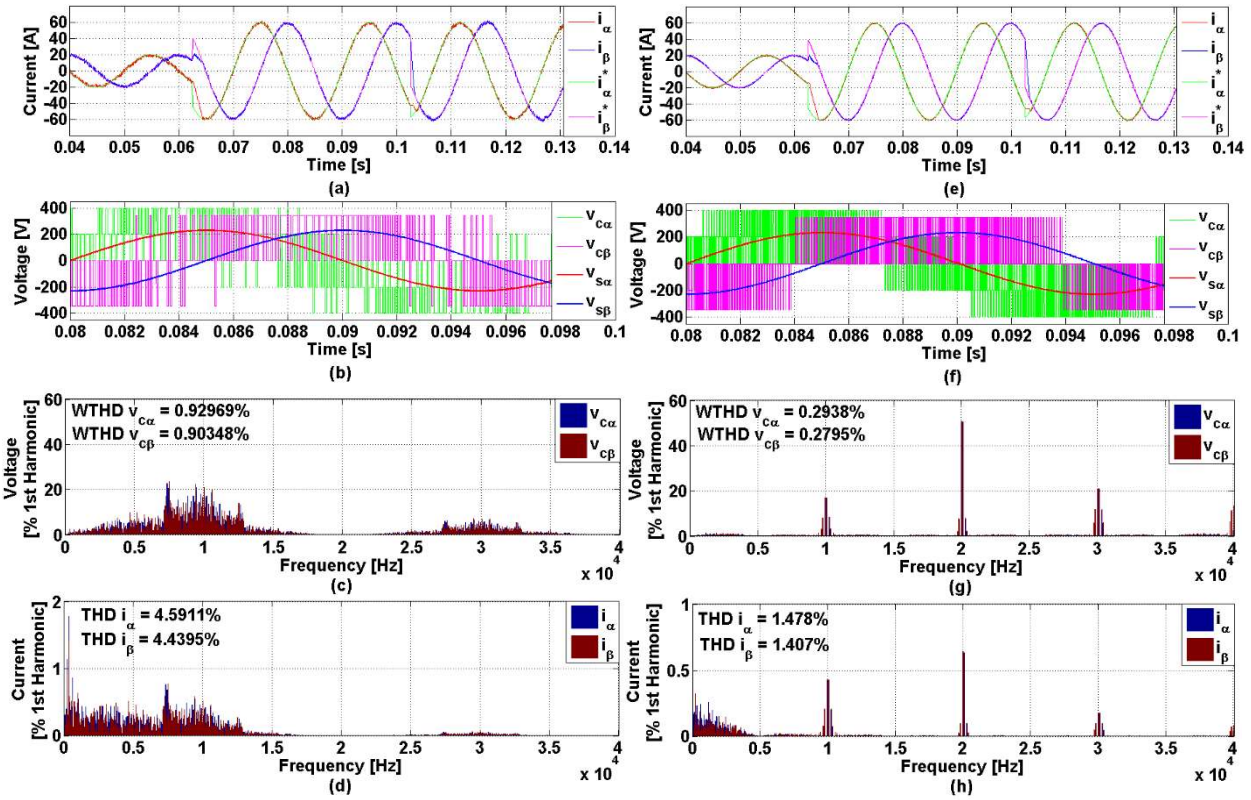

Figure 9. Simulation results for MPC (a-d) and M^{2}PC (e-h): Current tracking (a) (e), Supply and Converter voltages (b) (f), Converter voltage Harmonic contents (c) (g), Current Harmonic content (d) (h).

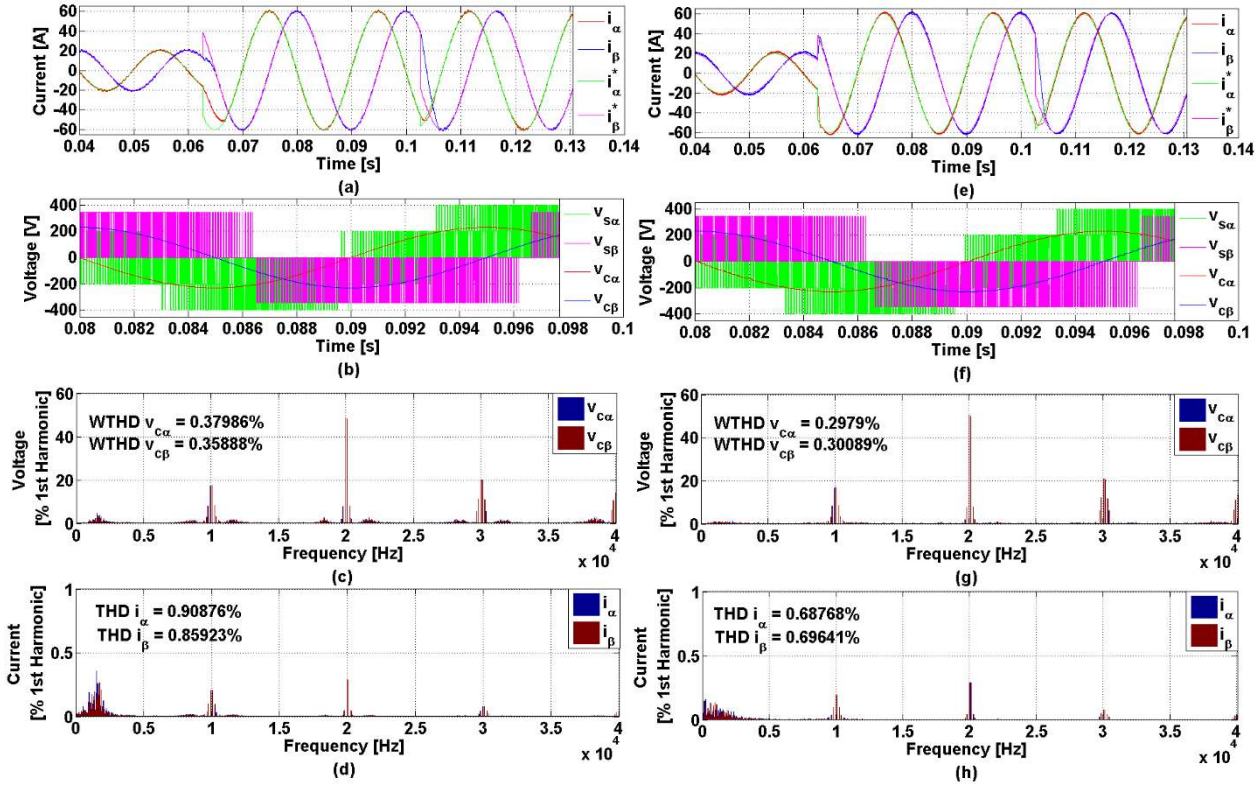

Figure 10. Simulation results for synchronous reference frame control (a-d) and DBC (e-h): Current tracking (a) (e), Supply and Converter voltages (b) (f), Converter voltage Harmonic contents (c) (g), Current Harmonic content (d) (h).

VII. EXPERIMENTAL RESULTS

Experimental tests has been carried out for MPC and M^{2}PC controllers using a low power inverter, shown in figure 11. The active rectifier configuration, shown in figure 1b, is considered in order to avoid the requirement of a high voltage DC source. A supply voltage of 70V peak is used in order to produce an avoid to exceed the load resistor rated power. The experimental parameters are shown in Table IV and in figure 9 the obtained results, for both MPC and M^{2}PC, are shown.

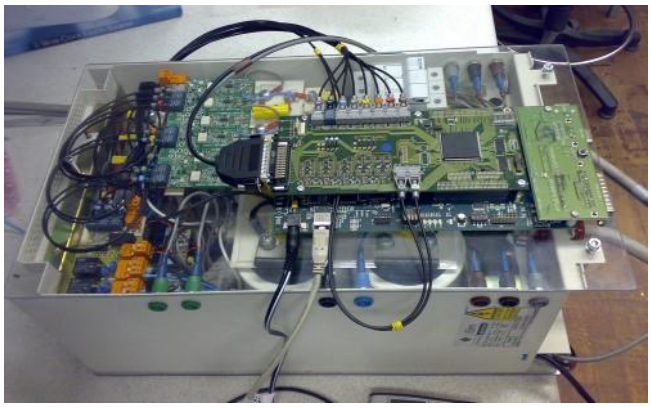

Figure 11. Experimental setup.

The currents produced by MPC, shown in Figure 12a, present a high harmonic content and less repetitive waveforms, compared with the current produced by M^{2}PC in figure 12f. In fact also with a sampling frequency of *20kHz* the MPC produce a considerable amount of harmonics at frequencies lower than *10kHz* with a *THD* around *8%*, as shown in figure 12b.

TABLE IV. EXPERIMENTAL PARAMETERS.

Name	Description	Value	Unit
L	Line Inductance	3	[mH]
r_l	Leakage Resistance	0.5	[Ω]
R	Load resistance	20/30	[Ω]
P_R	Load resistor rated power	1	[kW]
V_s	Supply Voltage peak value	70	[V]
I	Converted rated peak current	15	[A]
V_{DC}	DC-Link Voltage	2.2 V_s	[V]
f_s	Sampling Frequency	20 (MPC) 10(PI, DBC, M^{2}PC)	[kHz]
f_{sw}	Switching Frequency	~ 7 (MPC) 10 (PI, DBC, M^{2}PC)	[kHz]

M^{2}PC produces the typical spectrum of SVM, shown in figure 12i, with most parts of the harmonics are located around the switching frequency which in this case is equal to the sampling frequency and a *THD* around *3%*. Figure 12c and figure 12h show the supply voltages, respectively for MPC and M^{2}PC; due to the grid impedance, the low quality current produced by MPC inject harmonics on the supply voltage that results distorted. On the other hand, the currents produced by M^{2}PC does not affect the supply voltages due to their lower magnitude and higher frequency. The current tracking of MPC (figure 12d) and M^{2}PC (figure 12i) is also compared and both controllers effectively track the current reference with a fast response but M^{2}PC present a smoother current compared to MPC as expected. Finally the DC-Link voltage tracking of MPC (figure 12e) and M^{2}PC (figure 12j) is presented with both controllers regulating the DC-Link voltage effectively but, again MPC presents a slightly higher voltage ripple compared to M^{2}PC. From Figure 13, which shows the execution time for both MPC and M^{2}PC, it can be observed that approximately twice of the time is needed to execute M^{2}PC compared to MPC. However, considering the different sampling frequencies, both controllers need about 40% of the available time interval. Figure 14 shows M^{2}PC transient response to a variation in the DC load resistance from 30Ω to 20Ω (a-b) and to a current reference phase jump of 30° (c-d). The results shows that the M^{2}PC is able to track the current references with negligible errors; however, the dynamic response is limited by the DC-Link voltage control.

VIII. CONCLUSION

A Modulated Model Predictive Control (M^{2}PC) has been proposed in this paper and applied for the current control of a 2-Level, 3-Phase Active Front-End considering both inverter and active rectifier configurations. M^{2}PC differs from the classic MPC for the inclusion, inside the cost function minimization, of a suitable modulation scheme, such as the proposed SVM technique. The main advantage of M^{2}PC, compared with MPC, is the constant switching frequency and variable voltage pulse width. Simulations have been carried out considering the inverter configuration, showing the fast response to amplitude and phase steps of the current references of both controllers. The benefits of including a modulation scheme inside the predictive algorithm can be noticed; in fact M^{2}PC presents a current *THD* three times lower than the current *THD* produced by MPC. Moreover the current harmonic content of M^{2}PC is mainly located around the frequencies as multiple of f_s while, for MPC, a low frequency current harmonic content where the highest harmonics are at frequencies below $f_s/2$ is observed. Experimental testing has been carried out considering the active rectifier configuration in order to avoid the use of high-voltage DC sources, and validate the results obtained in simulation. The M^{2}PC retains all the desirable multi-objective control characteristics of MPC such as fast dynamic response, easy inclusion of nonlinearities and constraints with respect to traditional control techniques for power electronic converters, possibility of incorporating nested control loops in only one loop and the flexibility to include other system requirements in the controller. The possibility to modify the cost function of M^{2}PC in order to perform a multi-variable cost function minimization is currently under investigation and will be the subject of future research publications.

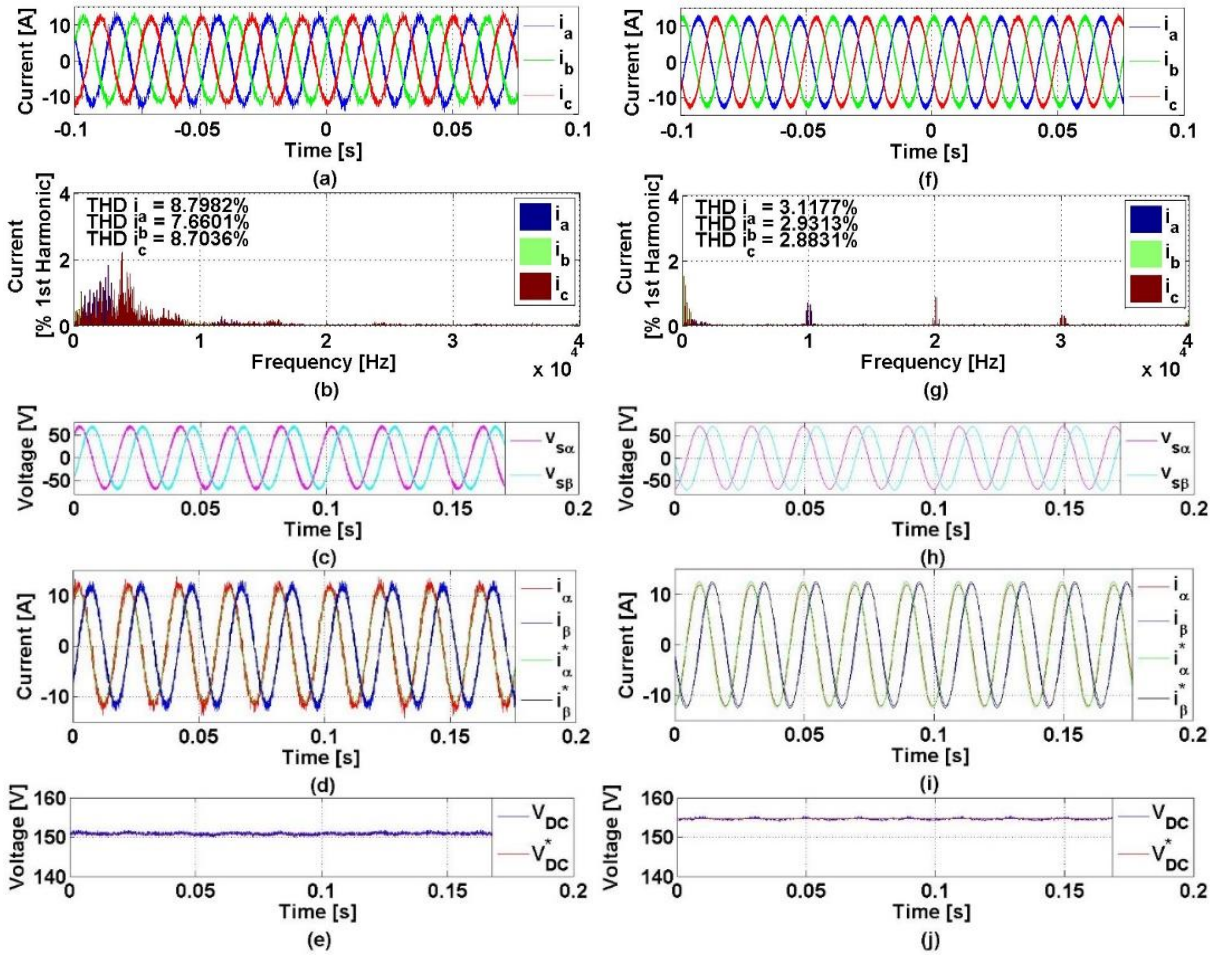

Figure 12. Experimental results for MPC (a-e) and M^{2}PC (f-j): AC current (a) (f), AC current harmonic content (b) (g), Supply voltages (c) (h), AC current tracking (d) (i), DC Link voltage tracking (e) (j).

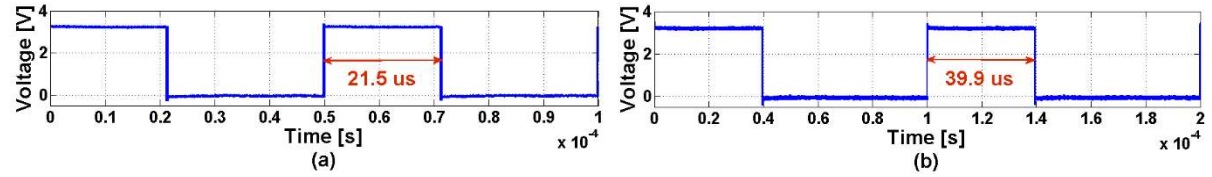

Figure 13. Measured code execution time for MPC (a) and M^{2}PC (b)

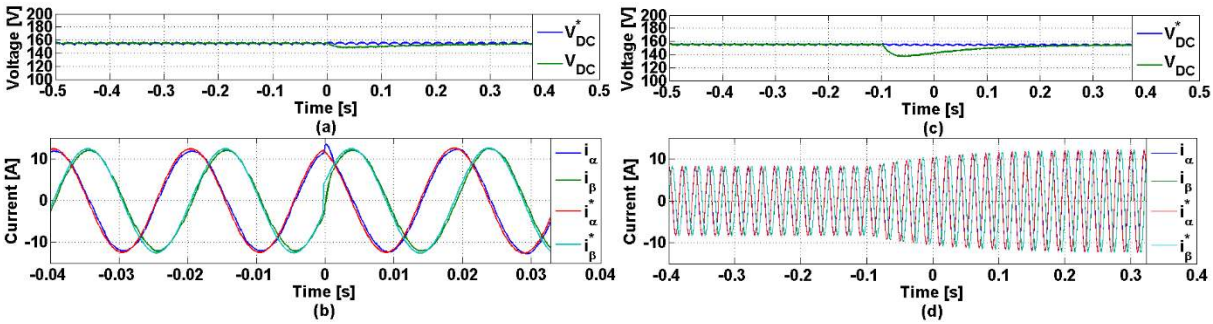

Figure 14. M^{2}PC transient response to a load variation from 20Ω to 30Ω (a-b) and to a current reference phase jump of 30° (c-d): (a), (c) DC-Link voltage, (c), (d) AC currents in static reference frame.

REFERENCES

[1] S. Kouro, P. Cortés, R. Vargas, U. Ammann, and J. Rodríguez, "Model predictive control—A simple and powerful method to control power converters," *IEEE Trans. Ind. Electron.*, vol. 56, no. 6, pp. 1826–1838, 2009.

[2] P. Zanchetta and P. Cortés, "Finite States Model Predictive Control for Shunt Active Filters," *IEEE Annu. Conf. Ind. Electron.*, pp. 581–586, 2011.

[3] J. Rodríguez, J. Pontt, and C. Silva, "Predictive current control of a voltage source inverter," *IEEE Trans. Ind. Electron.*, vol. 54, no. 1, pp. 495–503, 2007.

[4] P. Cortés and J. Rodríguez, "Predictive current control strategy with imposed load current spectrum," *IEEE Trans. Power Electron.*, vol. 23, no. 2, pp. 612–618, 2008.

[5] J. Rodriguez and P. Cortes, *Predictive Control of Power Converters and Electrical Drives*. Wiley-IEEE Press, 2012, pp. 1–230.

[6] J. Rodríguez, J. Pontt, C. Silva, M. Salgado, S. Rees, U. Ammann, P. Lezana, R. Huerta, and P. Cortés, "Predictive control of three-phase inverter," *IEE Electron. Lett.*, vol. 40, no. 9, pp. 561–562, 2004.

[7] S. Müller, U. Ammann, and S. Rees, "New Time-Discrete Modulation Scheme for Matrix Converters," *IEEE Trans. Ind. Electron.*, vol. 52, no. 6, pp. 1607–1615, 2005.

[8] F. Villarroel, J. R. Espinoza, C. A. Rojas, J. Rodríguez, M. Rivera, and D. Sbárbaro, "Multiobjective Switching State Selector for Finite-States Model Predictive Control Based on Fuzzy Decision Making in a Matrix Converter," *IEEE Trans. Ind. Electron.*, vol. 60, no. 2, pp. 589–599, 2013.

[9] R. Vargas, J. Rodríguez, U. Ammann, and P. W. Wheeler, "Predictive Current Control of an Induction Machine Fed by a Matrix Converter With Reactive Power Control," *IEEE Trans. Ind. Electron.*, vol. 55, no. 12, pp. 4362–4371, 2008.

[10] T. Geyer, G. Papafotiou, and M. Morari, "Model Predictive Direct Torque Control—Part I: Concept, Algorithm, and Analysis," *IEEE Trans. Ind. Electron.*, vol. 56, no. 6, pp. 1894–1905, Jun. 2009.

[11] G. Papafotiou, J. Kley, K. G. Papadopoulos, P. Bohren, and M. Morari, "Model Predictive Direct Torque Control—Part II: Implementation and Experimental Evaluation," *IEEE Trans. Ind. Electron.*, vol. 56, no. 6, pp. 1906–1915, Jun. 2009.

[12] G. Abad, M. Á. Rodríguez, and J. Poza, "Two-Level VSC Based Predictive Direct Torque Control of the Doubly Fed Induction Machine With Reduced Torque and Flux Ripples at Low Constant Switching Frequency," *IEEE Trans. Power Electron.*, vol. 23, no. 3, pp. 1050–1061, 2008.

[13] H. Miranda, P. Cortés, J. I. Yuz, and J. Rodríguez, "Predictive Torque Control of Induction Machines Based on State-Space Models," *IEEE Trans. Ind. Electron.*, vol. 56, no. 6, pp. 1916–1924, 2009.

[14] T. Geyer, N. Oikonomou, G. Papafotiou, and F. D. Kieferndorf, "Model Predictive Pulse Pattern Control," *IEEE Trans. Ind. Appl.*, vol. 48, no. 2, pp. 663–676, 2012.

[15] J. Hu and Z. Zhu, "Improved Voltage-Vector Sequences on Dead-Beat Predictive Direct Power Control of Reversible Three-Phase Grid-Connected Voltage-Sourced Converters," *IEEE Trans. Power Electron.*, vol. 28, no. 1, pp. 254–267, 2013.

[16] P. Antoniewicz and M. P. Kazmierkowski, "Virtual-Flux-Based Predictive Direct Power Control of AC/DC Converters With Online Inductance Estimation," *IEEE Trans. Ind. Electron.*, vol. 55, no. 12, pp. 4381–4390, Dec. 2008.

[17] R. Gregor, F. Barrero, S. Toral, M. J. Durán, M. R. Arahal, J. Prieto, and J. L. Mora, "Predictive-space vector PWM current control method for asymmetrical dual three-phase induction motor drives," *IET Electr. Power Appl.*, vol. 4, no. 1, p. 26, 2010.

[18] F. Barrero, M. R. Arahal, R. Gregor, S. Toral, and M. J. Durán, "One-Step Modulation Predictive Current Control Method for the Asymmetrical Dual Three-Phase Induction Machine," *IEEE Trans. Ind. Electron.*, vol. 56, no. 6, pp. 1974–1983, 2009.

[19] S. Vazquez, C. Montero, C. Bordons, and L. G. Franquelo, "Model predictive control of a VSI with long prediction horizon," *IEEE Int. Symp. Ind. Electron.*, pp. 1805–1810, Jun. 2011.

[20] P. Stolze, P. Landsmann, R. Kennel, and T. Mouton, "Finite-Set Model Predictive Control With Heuristic Voltage Vector Preselection For Higher Prediction Horizons," *Eur. Conf. Power Electron. Appl.*, 2011.

[21] N. D. Marks, T. J. Summers, and R. E. Betz, "Finite Control Set Model Predictive Control with Increased Prediction Horizon for a 5 Level Cascaded H-Bridge StatCom Model Predictive Control for Power Converters," *Eur. Conf. Power Electron. Appl.*, pp. 1–10, 2013.

[22] S. Vazquez, C. Montero, C. Bordons, and L. G. Franquelo, "Design and experimental validation of a Model Predictive Control strategy for a VSI with long prediction horizon," *IEEE Annu. Conf. Ind. Electron.*, pp. 5788–5793, Nov. 2013.

[23] L. Tarisciotti, P. Zanchetta, A. Watson, J. Clare, and S. Bifaretti, "Modulated Model Predictive Control for a 7-Level Cascaded H-Bridge back-to-back Converter," *IEEE Trans. Ind. Electron.*, vol. pp, no. 99, pp. 1–9, 2014.

[24] L. Tarisciotti, P. Zanchetta, A. J. Watson, J. C. Clare, S. Bifaretti, and M. Rivera, "A new Predictive Control method for cascaded multilevel converters with intrinsic modulation scheme," *IEEE Annu. Conf. Ind. Electron.*, pp. 5764–5769, 2013.

[25] S. Bifaretti, P. Zanchetta, and Y. Fan, "Power flow control through a multi-level H-bridge based power converter for Universal and Flexible Power Management in future electrical grids," *Int. Power Electron. Motion Control Conf.*, pp. 1771–1778, 2008.

[26] A. J. Watson and H. Dang, "Control challenges and solutions for a multi-cellular converter for use in electricity networks," *EPE J. Eur. Power Electron. Drives*, vol. 19, no. December, pp. 25–31, 2009.

[27] V. Biagini, M. Odavic, P. Zanchetta, M. Degano, and P. Bolognesi, "Improved dead beat control of a shunt active filter for aircraft power systems," in *IEEE International Symposium on Industrial Electronics (ISIE)*, 2010, pp. 2702–2707.

[28] S. Bifaretti, P. Zanchetta, A. J. Watson, L. Tarisciotti, and J. C. Clare, "Advanced power electronic conversion and control system for universal and flexible power management," *IEEE Trans. Smart Grid*, vol. 2, no. 2, pp. 231–243, 2011.

[29] M. Oettmeier, C. Heising, V. Staudt, and A. Steimel, "Dead-beat control algorithm for single-phase 50-kw AC railway grid representation," *IEEE Trans. Power Electron.*, vol. 25, no. 5, pp. 1184–1192, 2010.

[30] A. Bellini and S. Bifaretti, "Performances of a PLL based digital filter for double-conversion UPS," *Int. Power Electron. Motion Control Conf.*, pp. 490–497, 2008.

[31] L. Tarisciotti, A. J. Watson, P. Zanchetta, S. Bifaretti, J. C. Clare, and P. W. Wheeler, "An improved Dead-Beat current control for Cascaded H-Bridge active rectifier with low switching frequency," in *IET International Conference onPower Electronics, Machines and Drives (PEMD)*, 2012, pp. 1–6.

[32] P. Zanchetta and D. Gerry, "Predictive current control for multilevel active rectifiers with reduced switching frequency," *IEEE Trans. Ind. Electron.*, vol. 55, no. 1, pp. 163–172, 2008.

[33] C. Cecati, A. Dell'Aquila, M. Liserre, and V. G. Monopoli, "A passivity-based multilevel active rectifier with adaptive compensation for traction applications," *IEEE Trans. Ind. Appl.*, vol. 39, no. 5, pp. 1404–1413, 2003.